A Reconfigurable Photonic Microwave Mixer Using a 90° Optical Hybrid

Zhenzhou Tang, *Graduate Student Member, IEEE* and Shilong Pan, *Senior Member, IEEE*

***Abstract*— A reconfigurable photonic microwave mixer is proposed using a 90° optical hybrid. To perform the reconfigurable mixing, an optical carrier is split into two branches. One portion is intensity-modulated by an RF or intermediate frequency signal, and the other is driven by a local oscillator (LO). Each generates an optical sideband. The two sidebands from the two branches are introduced to the signal port and the LO port of an optical hybrid which typically has four output ports, namely, I_1, I_2, Q_1, and Q_2. When any one of the outputs is detected by a photodetector (PD), a single-ended mixer is obtained. If one of the combinations (I_1, I_2) and (Q_1, Q_2) is sent to a balanced PD, a balanced mixer is realized. When I_1 (or I_2) and Q_1 (or Q_2) are detected by two PDs, an I/Q mixer with quadrature outputs is achieved. When an electrical 90° hybrid is used to combine the two outputs of the I/Q mixer, image-reject mixing is implemented. A theoretical model is established to analyze the proposed mixer, and an experiment is also carried out. The results demonstrate that the proposed mixer can achieve reconfigurable mixing functions by simply changing the photodetection method.**

***Index Terms*— Balanced mixer, image reject, microwave photonics, mixer, optical hybrid.**

I. Introduction

A FREQUENCY mixer, which is used to upconvert a baseband or intermediate frequency (IF) signal to the RF band, or to downconvert an RF signal to the IF band, is regarded as an important module in microwave systems. Compared with the electrical mixer, the microwave photonic frequency converter becomes more and more popular because of its advantages of broad bandwidth, high RF, and local oscillator (LO) isolation and immunity to electromagnetic interference [1]. Besides, the low transmission loss and light weight of the optical components, especially the optical fiber, make the photonic microwave mixer more attractive for some applications in harsh environments, for instance, the avionics [2], radar receiver [3], and satellite payloads [4], [5].

Manuscript received September 1, 2015; revised November 23, 2015 and July 12, 2016; accepted July 23, 2016. Date of publication August 11, 2016; date of current version September 1, 2016. This work was supported in part by the National Basic Research Program of China under Grant 2012CB315705, in part by the National Natural Science Foundation of China under Grant 61422108 and Grant 61527820, in part by the Fundamental Research Funds for the Central Universities, in part by the Project Funded by the Priority Academic Program Development of Jiangsu Higher Education Institutions, and in part by the Funding for Outstanding Doctoral Dissertation in NUAA under Grant BCXJ16-04.

The authors are with the Key Laboratory of Radar Imaging and Microwave Photonics, Ministry of Education, Nanjing University of Aeronautics and Astronautics, Nanjing 210016, China (e-mail: pans@ieee.org).

Color versions of one or more of the figures in this paper are available online at http://ieeexplore.ieee.org.

Digital Object Identifier 10.1109/TMTT.2016.2594278

It is well known that frequency mixing is an effect caused by nonlinearity. Based on different nonlinear media, various efforts have been studied to perform photonic mixing in the literature. For example, a semiconductor laser can be used to perform photonic frequency mixing [6]. Since the bandwidth of the laser diode (LD) is usually small, this kind of mixer can only be applied when the RF is low. The semiconductor optical amplifier (SOA) is also a promising device to realize photonic frequency mixing, thanks to the strong nonlinear effects, such as cross-phase modulation [7], four-wave mixing [8], cross-gain modulation [9], and cross-polarization modulation [10]. The major problem associated with SOA-based methods is the poor quality of the converted signal. The nonlinearity in an electro-optical modulator was also applied to implement photonic frequency mixing [11], [12]. From then on, considerable efforts have been devoted to study the external-modulator-based photonic frequency mixing thanks to the relatively large bandwidth and well-controlled nonlinearity of the electro-optical modulators [13]–[22]. The most common architecture of the external-modulator-based photonic mixer is constructed by connecting two optical modulators in series [13]. The key advantage of this approach is the ultrahigh isolation since the RF and LO signals are introduced to different modulators. However, it has two main drawbacks of low conversion efficiency (due to the large insertion loss of the cascaded modulators) and large mixing spurs (generated by the frequency beating within the useless sidebands). To increase the conversion efficiency, a carrier-suppressed modulation scheme followed by optical amplification can be applied [14]–[16], and to reduce the mixing spurs, the undesirable sidebands are removed by optical filters (OFs) [17], [18]. The reduction of the spurious and the improvement of the conversion efficiency can be simultaneously achieved based on a dual-drive Mach–Zehnder modulator (MZM) [21], [22], which has no LO and RF leakages thanks to the elimination of the optical carrier.

Although photonic frequency mixing has been studied for nearly three decades, most of the implementations only achieve the fundamental mixing function, i.e., single-ended mixing, and many other advanced frequency mixers have rarely been realized, such as the balanced-mixer (double-balanced or triple-balanced mixer), I/Q mixer (also called quadrature mixer), and image-reject mixer (or single-sideband mixer). Compared with the single-ended mixer, the balanced mixer can suppress the dc components and reduce spurious mixing [23]; the I/Q mixer (or quadrature mixer) could achieve a phase-irrelevant frequency conversion, which produces

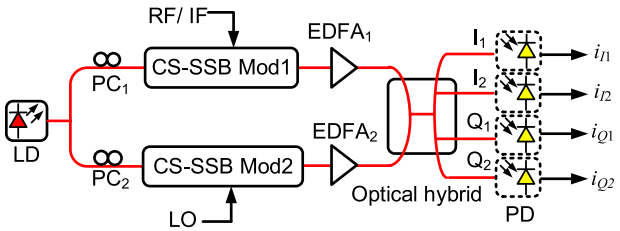

Fig. 1. Schematic of the reconfigurable mixer. LD: laser diode. PC: polarization controller. CS-SSB Mod: carrier-suppressed single sideband modulator. MZM: Mach–Zehnder modulator. OF: optical filter. EDFA: erbium-doped fiber amplifier. ESA: electrical spectrum analyzer. PD: photodetector.

two quadrature signals; and the image-reject mixer (usually used for downconversion) can avoid interference from the spurious signals at the image frequency [24]. Previously, a photonic I/Q downconverter using a parallel phase-modulation structure was proposed in [25], but quadrature LO signals are needed to obtain the quadrature outputs. The photonic image-reject mixers were also demonstrated [26]–[28]. In [26] and [27], two exact quadrature LO signals are also required to achieve an acceptable image-reject ratio (IRR), while in [28] multiple conversion stages together with prefiltering are employed, resulting in a complex and bulky system. Recently, we have reported a reconfigurable frequency mixer using an optical 90° hybrid, which can implement all the aforementioned mixing functions [29], but only some preliminary experimental observations have been reported.

In this paper, a more comprehensive study of the reconfigurable photonic mixer using a 90° optical hybrid is carried out. A detailed theoretical analysis and experimental demonstrations are carried out. Seen from the results, this frequency mixer has three distinguishing features.

1) Single-ended, double-balanced, I/Q, and image-reject mixing can be obtained by changing the detection scheme to the outputs of the optical hybrid.
2) The signals applied to the photodetectors (PDs) only contain the necessary first-order sidebands, so the mixing spurs and the RF/IF and LO leakages generated by the frequency beating between the useless sidebands can be highly suppressed, i.e., no electrical filter is needed to select the desired signal, which ensures a multioctave operational frequency range.
3) Compared with the conventional quadrature and image-reject mixers based on the electrical 90° hybrid coupler, the stage for the generation of exactly quadrature LOs is not required due to the use of the 90° optical hybrid, which ensures broadband operation and simple configuration.

The principle analysis of the reconfigurable mixer is presented in Section II. In Section III, an experiment is carried out to verify the performance and the results are also shown. In Section IV, some discussions are provided, and a conclusion is drawn in Section V.

II. Analysis

A. Principle

Fig. 1 shows the schematic of the reconfigurable mixer. An optical carrier generated by an LD is split into two equal branches by an optical coupler. The optical carrier in the upper branch is sent to a carrier-suppressed single sideband modulator (CS-SSB Mod1) via a polarization controller (PC, PC_1). An RF or IF signal is sent to the RF port CS-SSB Mod1. The CS-SSB Mod1 can be implemented by a conventional intensity or phase modulator together with an optical bandpass filter or a commercially available dual-parallel MZM (DPMZM) [29]. Due to the CS-SSB modulation, only one of the first-order sidebands would be generated. For simplicity, we assume that the negative first-order sideband is obtained, so the optical signal in the upper branch can be written as

$$E_S = -\sqrt{\frac{P_{\text{in}}}{2}}\sqrt{t_{\text{ff1}}}\sqrt{G_1}J_1(\beta_S)\exp[j(\omega_c-\omega_S)t] \quad (1)$$

where ω_c and P_{in} are the angular frequency and power of the optical carrier, ω_S is the angular frequency of the RF/IF signal, G_1 is the gain of erbium-doped fiber amplifier (EDFA_1), J_1 represents the first-order Bessel function of the first kind, β_S is the modulation index, V_S is the amplitude of the RF/IF signal, and t_{ff1} is the insertion loss of CS-SSB Mod1.

The optical carrier in the lower branch is sent to a second CS-SSB modulator (CS-SSB Mod2) via PC_2, which is then modulated by an LO. After amplified by the lower EDFA (EDFA_2), the output signal is expressed as

$$E_L = \pm\sqrt{\frac{P_{\text{in}}}{2}}\sqrt{t_{\text{ff2}}}\sqrt{G_2}J_1(\beta_L)\exp[j(\omega_c\pm\omega_L)t] \quad (2)$$

where ω_L is the frequency of the LO, G_2 is the gain of EDFA_2, β_L is the modulation index of CS-SSB Mod2, and t_{ff2} is the insertion loss of CS-SSB Mod2. To implement frequency downconversion or upconversion, CS-SSB Mod2 should be able to produce either negative or positive first-order sideband.

Then, the signal in (1) is sent to the signal port of the 90° optical hybrid, and the optical signal in (2) is introduced to the LO port of the optical carrier. Four output signals from the four output ports of the optical hybrid can be obtained,

$$\begin{aligned}
I_1 &= \sqrt{\frac{P_{\text{in}}}{2}}[-\sqrt{t_{\text{ff1}}}\sqrt{G_1}J_1(\beta_S)\exp[j(\omega_c-\omega_S)t] \\
&\quad \pm\sqrt{t_{\text{ff2}}}\sqrt{G_2}J_1(\beta_L)\exp[j(\omega_c\pm\omega_L)t]] \\
I_2 &= \sqrt{\frac{P_{\text{in}}}{2}}[-\sqrt{t_{\text{ff1}}}\sqrt{G_1}J_1(\beta_S)\exp[j(\omega_c-\omega_S)t] \\
&\quad \mp\sqrt{t_{\text{ff2}}}\sqrt{G_2}J_{\pm1}(\beta_L)\exp[j(\omega_c\pm\omega_L)t]] \\
Q_1 &= \sqrt{\frac{P_{\text{in}}}{2}}[-\sqrt{t_{\text{ff1}}}\sqrt{G_1}J_1(\beta_S)\exp[j(\omega_c-\omega_S)t] \\
&\quad \pm j\sqrt{t_{\text{ff2}}}\sqrt{G_2}J_{\pm1}(\beta_L)\exp[j(\omega_c\pm\omega_L)t]] \\
Q_2 &= \sqrt{\frac{P_{\text{in}}}{2}}[-\sqrt{t_{\text{ff1}}}\sqrt{G_1}J_1(\beta_S)\exp[j(\omega_c-\omega_S)t] \\
&\quad \mp j\sqrt{t_{\text{ff2}}}\sqrt{G_2}J_{\pm1}(\beta_L)\exp[j(\omega_c\pm\omega_L)t]] \quad (3)
\end{aligned}$$

where $I_{1,2}$ denote the in-phase outputs and $Q_{1,2}$ represent the quadrature outputs.

If each of the output signals is directed into a PD, the generated photocurrents can be given by

$$\begin{aligned} i_{I_1} &= \mp\frac{P_{\text{in}}}{2}\Re\sqrt{t_{\text{ff1}}t_{\text{ff2}}}\sqrt{G_1G_2}J_1(\beta_S)J_1(\beta_L)\cos(\omega_S \pm \omega_L)t \\ i_{I_2} &= \pm\frac{P_{\text{in}}}{2}\Re\sqrt{t_{\text{ff1}}t_{\text{ff2}}}\sqrt{G_1G_2}J_1(\beta_S)J_1(\beta_L)\cos(\omega_S \pm \omega_L)t \\ i_{Q_1} &= \pm\frac{P_{\text{in}}}{2}\Re\sqrt{t_{\text{ff1}}t_{\text{ff2}}}\sqrt{G_1G_2}J_1(\beta_S)J_1(\beta_L)\sin(\omega_S \pm \omega_L)t \\ i_{Q_2} &= \mp\frac{P_{\text{in}}}{2}\Re\sqrt{t_{\text{ff1}}t_{\text{ff2}}}\sqrt{G_1G_2}J_1(\beta_S)J_1(\beta_L)\sin(\omega_S \pm \omega_L)t \end{aligned} \tag{4}$$

where $\Re$ denotes the responsivity of the PD.

As can be seen from (4), all the outputs contain the component at the mixing frequencies of $\omega_S \pm \omega_L$, so each of them can be functioned to be the simplest single-ended frequency mixer. Since i_{I1} and i_{I2} or i_{Q1} and i_{Q2} are out of phase, if a balanced PD is used, balanced frequency mixing can be achieved. In addition, considering that a quadrature phase difference exists between the in-phase outputs (i_{I1} and i_{I2}) and the quadrature outputs (i_{Q1} and i_{Q2}), a frequency I/Q mixer can also be realized. When two outputs of the I/Q mixer are quadraturely combined by an electrical quadrature hybrid coupler, an image-reject mixer for frequency downconversion could be obtained.

To explain the image rejection downconversion, an image is applied to CS-SSB Mod1 together with the useful RF signal. Then, the optical signal output from the upper branch can be expressed as

$$\begin{aligned} E_s' = \sqrt{\frac{P_{\text{in}}}{2}}[&-\sqrt{t_{\text{ff1}}}\sqrt{G_1}J_1(\beta_S)\exp[j(\omega_c - \omega_J)t] \\ &- \sqrt{t_{\text{ff1}}}\sqrt{G_1}J_1(\beta_S)\exp[j(\omega_c - \omega_S)t]] \end{aligned} \tag{5}$$

where $\omega_J = \omega_L - \omega_{\text{IF}}$ the angular frequency of the image. In this case, i_{I1} and i_{Q1} in (4) can be rewritten as

$$\begin{aligned} i_{I_1}' &= \frac{P_{\text{in}}}{2}\Re\sqrt{t_{\text{ff1}}t_{\text{ff2}}}\sqrt{G_1G_2}J_1(\beta_S)J_1(\beta_L) \\ &\quad\times[\cos(\omega_L - \omega_J)t + \cos(\omega_S - \omega_L)t] \\ i_{Q_1}' &= \frac{P_{\text{in}}}{2}\Re\sqrt{t_{\text{ff1}}t_{\text{ff2}}}\sqrt{G_1G_2}J_1(\beta_S)J_1(\beta_L) \\ &\quad\times[\sin(\omega_L - \omega_J)t - \sin(\omega_S - \omega_L)t]. \end{aligned} \tag{6}$$

When the signals in (6) are quadraturely combined and considering that $\omega_S - \omega_L = \omega_L - \omega_J = \omega_{\text{IF}}$, we get

$$\begin{aligned} i_{\text{IF}} &= \frac{P_{\text{in}}}{2}\Re\sqrt{t_{\text{ff1}}t_{\text{ff2}}}\sqrt{G_1G_2}J_1(\beta_R)J_1(\beta_L) \\ &\quad\times\left[\sin\left(\omega_L - \omega_J - \frac{\pi}{2}\right)t + \cos(\omega_L - \omega_J)t\right. \\ &\quad\left. + \cos(\omega_S - \omega_L)t - \sin\left(\omega_S - \omega_L - \frac{\pi}{2}\right)t\right] \\ &= P_{\text{in}}\Re\sqrt{t_{\text{ff1}}t_{\text{ff2}}}\sqrt{G_1G_2}J_1(\beta_R)J_1(\beta_L)\cos(\omega_S - \omega_L)t. \end{aligned} \tag{7}$$

The unwanted component at the frequency of $\omega_L - \omega_J$, as can be seen from (7), is significantly removed, i.e., the image rejection is realized.

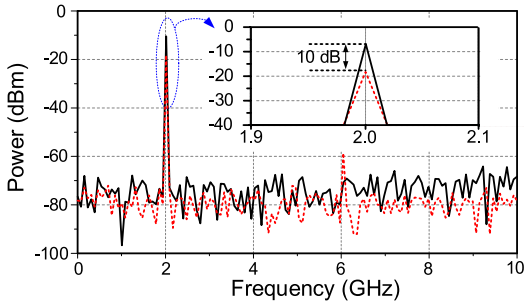

Fig. 2. Simulated electrical spectra of the proposed reconfigurable photonic microwave mixer (solid line) and the conventional cascaded-MZM-based photonic microwave mixer (dashed line) using Optisystem software. Inset: zoomed-in view of the peaks.

B. Conversion Efficiency

Taking the single-ended frequency mixer realized using the proposed scheme for frequency downconversion as an example, using an approximate expansion of the Bessel function with $J_1(\beta_S) \approx \beta_S/2$, i_{I1} can be rewritten as

$$i_{\text{IF}} = \frac{P_{\text{in}}}{4}\Re\sqrt{t_{\text{ff1}}t_{\text{ff2}}}\sqrt{G_1G_2}\beta_S J_{-1}(\beta_L)\cos(\omega_S - \omega_L)t. \tag{8}$$

Then the conversion efficiency can be expressed as

$$\eta = \frac{P_{\text{in}}^2}{16}\Re^2 t_{\text{ff1}}t_{\text{ff2}}G_1G_2\left(\frac{\pi}{V_{\pi 1}}\right)^2[J_{-1}(\beta_L)]^2 R_{\text{in}}R_{\text{out}} \tag{9}$$

where R_{in} is the equivalent input resistance of the modulator and R_{out} is the equivalent load resistance of the PD. Seen from (9), the conversion efficiency of the reconfigurable mixer is proportional to the multiplication of the gains of the two EDFAs, i.e., G_1G_2. Therefore, an effective way to improve the conversion efficiency is to increase the gain of the EDFAs.

For comparison, the conversion efficiency of the conventional photonic frequency downconverter based on cascaded intensity modulators [10] biased at quadrature point is given by

$$\eta' = \frac{P_{\text{in}}^2}{16}\Re^2 t_{\text{ff}}^2 G_{\text{EDFA}}^2\left(\frac{\pi}{V_\pi}\right)^2 J_1(\beta_L)^2 R_{\text{in}}R_{\text{out}} \tag{10}$$

where P_{in} is the optical power of the optical carrier, t_{ff} is the insertion loss, and G_{EDFA} is the gain of the optical amplifier.

In the proposed mixer, only two useful first-order sidebands are introduced to the PD, and the optical carrier which always has the largest power is suppressed. This means, for the same incident power to the PD, $t_{\text{ff1}}t_{\text{ff2}}G_1G_2$ in the proposed mixer would be much higher than $(t_{\text{ff}}G_{\text{EDFA}})^2$ in the conventional mixer based on cascaded MZMs. As a result, the conversion efficiency of the proposed mixer would be preferable.

The simulated conversion efficiencies of the proposed mixer and the conventional photonic microwave mixer [13] based on Optisystem software is shown in Fig. 2. Assuming that for both the mixers, the average power of the optical signal applied to the PD is 10 dBm, the power of the IF signal outputs from the proposed mixer is 10 dB higher than that of the IF signal outputs from the conventional photonic microwave mixer based on cascaded MZMs, as can be seen from the zoomed-in view of the peaks in Fig. 2, confirming that the proposed reconfigurable mixer has a higher conversion efficiency.

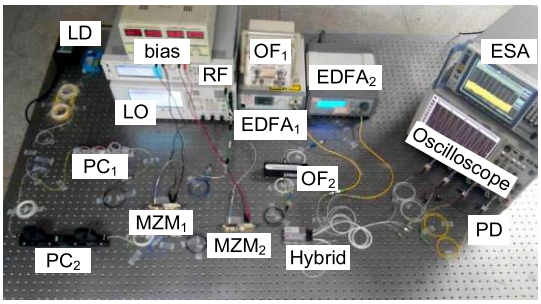

Fig. 3. Photograph of the experimental setup.

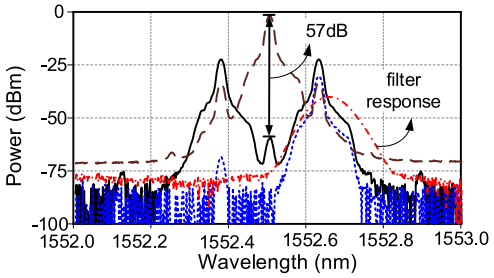

Fig. 4. Measured optical spectra of the signals in the upper branch.

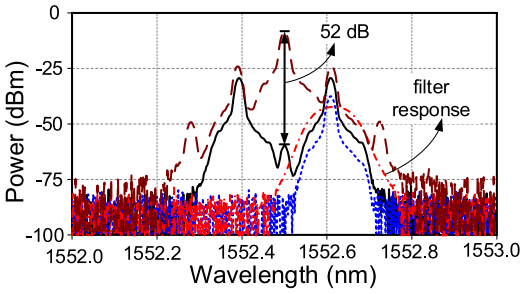

Fig. 5. Measured optical spectra of the signals in the lower branch when implementing frequency downconversion.

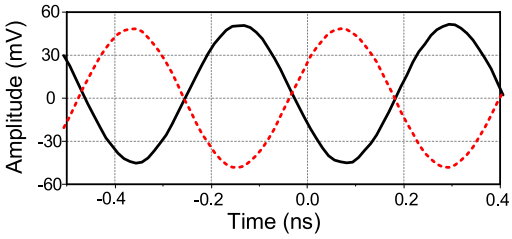

Fig. 6. Measured waveforms of i_{I1} (dashed line) and i_{I2} (solid line) for the double-balanced mixer when the IF signal is 2.29 GHz.

III. Experiment and Results

A. System Structure

Based on the schematic diagram in Fig. 1, an experiment is carried out. Fig. 3 presents the photograph of the experimental setup. A lightwave with a wavelength of 1552.5 nm and a power of 18 dBm is generated by an LD (Teraxion Inc.) and divided into two equal parts. Each branch has a CS-SSB modulator and an EDFA. The CS-SSB modulator is implemented by an MZM (MZM_1 and MZM_2) and an OF (OF_1 and OF_2). The bandwidth of the MZM is 40 GHz and the half-wave voltage is less than 4 V. OF_1 in CS-SSB Mod1 is realized by a commercially available programmable optical filter (Finisar 4000s) and OF_2 in CS-SSB Mod2 is performed by a tunable optical bandpass filter (Yenista XTM-50). RF signal is generated by a vector signal generator (Agilent E8267D) and an analog signal generator (Agilent E8257D) is used to generate the LO. The two branches are combined by a 90° optical hybrid (Kylia COH28). An optical spectrum analyzer (YOKOGAWA AQ6370C) and a 43-GHz electrical spectrum analyzer (Agilent N9030A) are used to measure the optical and electrical spectra, respectively. To observe the electrical waveform, a 32-GHz four-channel digital oscilloscope (Agilent DSO-X 92504A) is also used.

B. Frequency Downconversion

To achieve the frequency downconversion, negative first-order RF and LO sidebands should be obtained in the upper and lower branches, respectively. To do so, the MZM in the CS-SSB modulator is first biased at the carrier-suppression double-sideband (CS-DSB) condition. Then, the negative first-order sideband is selected by the optical bandpass filter. Fig. 4 depicts the optical spectra measured at the upper branch. The driving signal is a 5-dBm RF signal with a frequency of 16 GHz. The dashed line and the solid line show the optical spectra before and after carrier suppression, respectively. As can be seen, the optical carrier is suppressed by 57 dB due to the CS-DSB modulation, and the negative first-order sideband (shown as the short-dashed line) is selected by the optical bandpass filter, whose transmission response is plotted as the dashed-dotted line. Although a very small positive first-order sideband can be observed, it has a relatively low power, which can be neglected. Fig. 5 shows the optical spectra measured from the lower branch. LO frequency is 13.71 GHz and power is 5 dBm. Similarly, through the CS-DSB modulation realized by the MZM in CS-SSB Mod2, the optical carrier is suppressed by 52 dB (solid line). The dashed–dotted line in Fig. 5 is the filter response. With the assistance of the filter, the negative first-order LO sideband is selected, while the positive first-order sideband is almost fully suppressed.

The two signals from the two branches are amplified by the EDFAs, and introduced to the optical hybrid as the signal input and LO input. Four PDs (30 GHz, 0.85 A/W) are connected to the four outputs of the optical hybrid. Fig. 6 shows the measured waveforms of i_{I1} and i_{I2}. The waveforms of i_{I1} (dashed line) and i_{I2} (solid line) have identical amplitudes but opposite phases. According to the definition of the balanced mixer, a double-balanced mixer is obtained.

Similarly, seen from the waveforms plotted in Fig. 7, i_{I1} (dashed line) and i_{Q1} (solid line) have the same amplitudes with, however, a phase difference of $\pi/2$, indicating that an I/Q mixer with quadrature outputs is realized.

Using a commercially available electrical 90° hybrid (Krytar 3017360K, 1.7–36 GHz) to combine i_{I1} and i_{Q1}, the electrical waveform of the combined signal and the

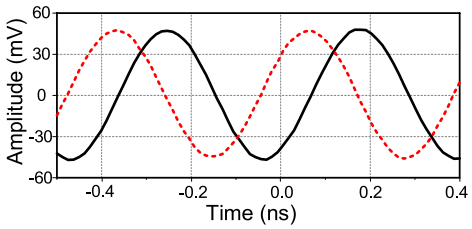

Fig. 7. Measured waveforms of i_{I1} (dashed line) and i_{Q1} (solid line) for the I/Q mixer when the IF signal is 2.29 GHz.

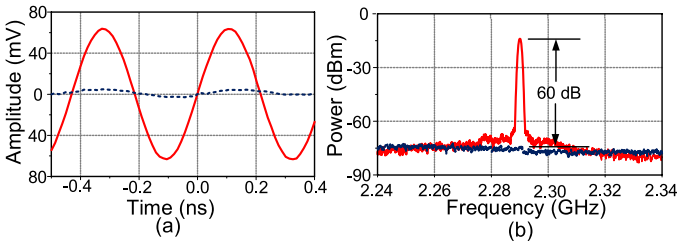

Fig. 8. Measured (a) waveforms and (b) spectra of the downconverted IF (solid line) and image (dashed line) signals from the image-reject mixer when the IF signal is 2.29 GHz.

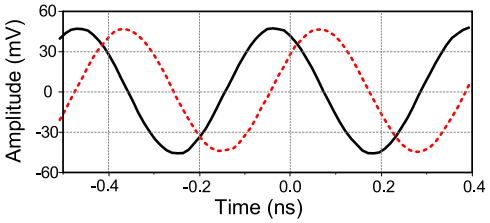

Fig. 9. Measured waveforms of i_{I1} (dashed line) and i_{Q1} (solid line) of the photonic microwave I/Q mixer when the image is applied.

corresponding spectrum are depicted as solid lines in Fig. 8(a) and (b), respectively. A 2.29 GHz IF signal with a power of −15 dBm is generated. To demonstrate the image rejection performance, an image at a frequency of 11.42 GHz is introduced to the proposed mixer. Fig. 9 shows the measured waveforms of i_{Q1} and i_{I1} in this case. Compared with the waveforms in Fig. 7, the two outputs are still quadrature, but i_{Q1} is phase shifted by π. The measured electrical waveform of the obtained downconverted image is marked as a dashed line in Fig. 8(a), when the two outputs are quadraturely combined by the same IF quadrature hybrid. The amplitude of the downconverted image is nearly zero. Seen from the corresponding electrical spectrum shown as the dashed line in Fig. 8(b), the downconverted image is less than −75 dBm. This means, the IRR is more than 60 dB, which is higher than most of the commercially available electrical image-rejected mixers (typically ∼30 dB).

Fig. 10(a) shows the downconversion efficiency when the RF power is increased. As can be seen, the IF power increases linearly with the RF power at different LO powers. When the LO power is 10 dBm, the conversion efficiency that can be found from the slope of the curve is about −10 dB. Fig. 10(b) shows the relationship between the IF power and the LO power. Again, a linear relationship is observed.

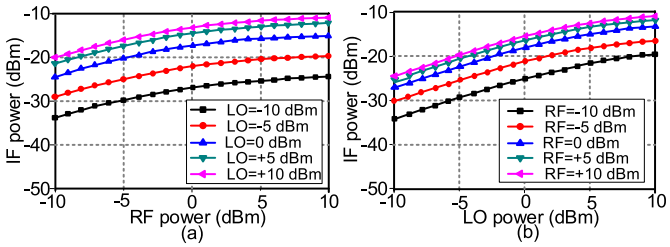

Fig. 10. Measured electrical power of the IF signal versus the (a) RF power and (b) LO power.

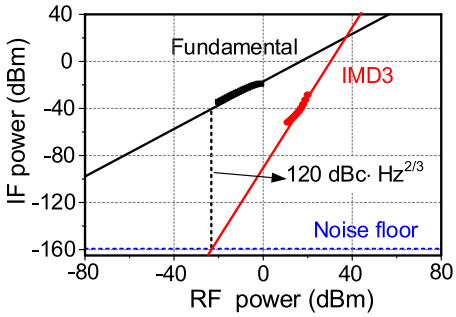

Fig. 11. Measured powers of the fundamental and IMD3 components versus the power of the input two-tone RF signal.

The mixing distortion of the mixer is also evaluated. It is well known that if a two-tone RF signal at the frequencies of ω_{S1} and ω_{S2} are applied to the photonic frequency mixer, various distortions will be generated. Among all the distortions, the third-order intermodulation distortions (IMD3) at the frequencies of $(2\omega_{S1}-\omega_{S2})\pm\omega_L$ and $(2\omega_{S2}-\omega_{S1})\pm\omega_L$ are the most harmful ones, as they are usually very close to the desired IF signal and cannot be removed by electrical filters. The spurious free dynamic range (SFDR) of the proposed photonic microwave mixer is measured by introducing a two-tone RF signal with frequencies of 16 and 16.02 GHz to its upper branch. The powers of the fundamental and IMD3 components versus the power of the input two-tone RF signal are shown in Fig. 11. If a noise floor at -160 dBm/Hz is assumed, the calculated SFDR is about 120 dBc·Hz$^{2/3}$, which confirms that the mixing distortion of the mixer is well suppressed.

Then, the RF and LO frequencies are changed to obtain IF signals at different frequencies. Fig. 12 shows the measured electrical spectra of the downconverted IF signals when the LO frequency is fixed at 16 GHz and a 17–33 GHz RF signal is applied to the proposed mixer. As can be seen, wideband frequency downconversion can be realized. Without the use of any electrical filter at the end of the PD, the LO and RF leakages and other mixing spurs are fully suppressed. Besides, only the downconversion is achieved, and the sum-frequency component, which is usually difficult to be removed for the conventional electrical and photonic frequency mixers, are eliminated.

C. Frequency Upconversion

To achieve frequency upconversion, the positive first-order sideband is selected by changing the center wavelength of OF_2

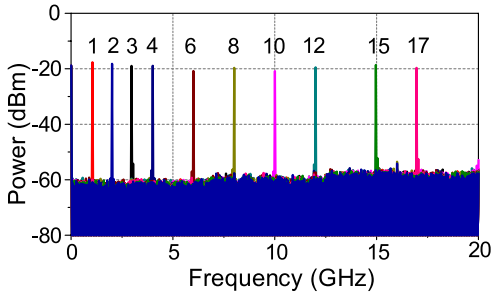

Fig. 12. Measured spectra of the downconverted IF signals when the LO frequency is fixed at 16 GHz and the RF is tuning from 17 to 33 GHz.

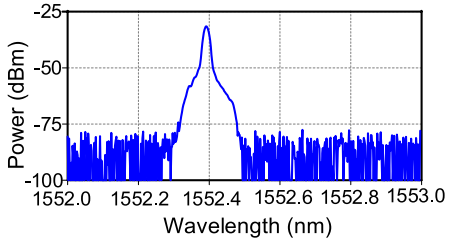

Fig. 13. Measured optical spectrum of the signal in the lower branch when implementing frequency upconversion.

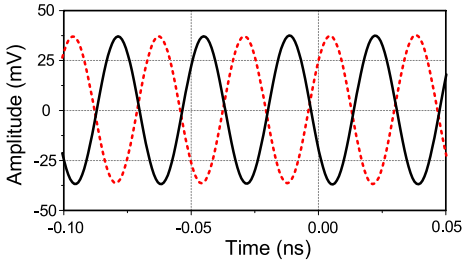

Fig. 14. Measured waveforms of i_{I1} (dashed line) and i_{I2} (solid line) for the double-balanced mixer when the upconverted signal is 29.71 GHz.

in the lower branch. Fig. 13 shows the optical spectrum of the selected sideband. The 16-GHz signal in the upper branch, in this case, is viewed as the IF input. Fig. 14 shows the electrical waveforms of i_{I1} and i_{I2}. As can be seen, the frequency upconversion is realized, and the two frequency components have a phase difference of π. Therefore, a double-balanced frequency upconverter is achieved. The waveforms of the i_{I1} and i_{Q1} are also measured and shown in Fig. 15. The two waveforms have a quadrature phase difference, indicating a quadrature frequency upconverter is achieved.

The upconversion efficiency of the proposed photonic frequency mixer is studied. As can be seen from Fig. 16(a), a linear relationship between the upconverted signal power and the input IF power is observed. A similar result can be seen from Fig. 16(b). Fig. 17 shows the SFDR performance of the frequency upconverter. The measured SFDR of the proposed reconfigurable mixer when working in the upconversion mode is about 116 dBc $\cdot$ Hz$^{2/3}$.

If the IF is adjusted from 1 to 15 GHz and the LO frequency is fixed at 16 GHz, a tunable frequency upconversion

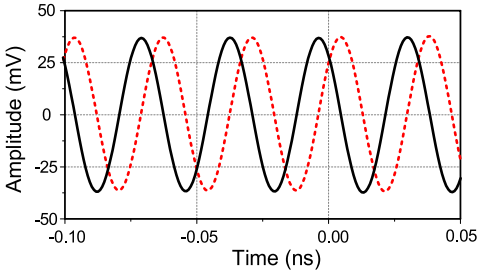

Fig. 15. Measured waveforms of i_{I1} (dashed line) and i_{Q1} (solid line) for the I/Q mixer when the upconverted signal is 29.71 GHz.

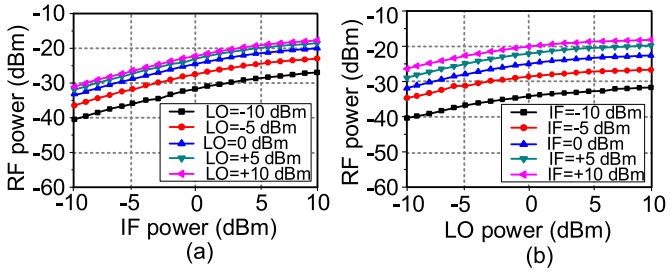

Fig. 16. Measured power of the upconverted signal versus the (a) IF power and (b) LO power.

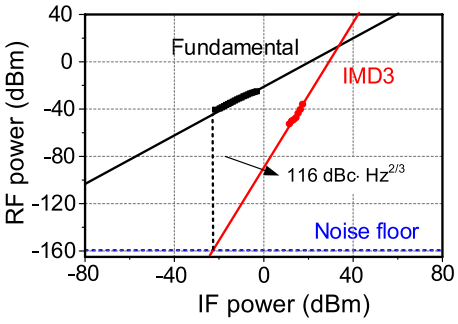

Fig. 17. Powers of the fundamental and IMD3 components versus the input two-tone IF signal power.

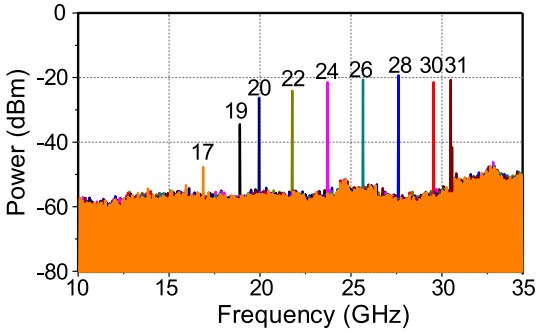

Fig. 18. Measured electrical spectra of the upconverted signals when the LO frequency is fixed at 16 GHz and the IF is tuned from 1 to 15 GHz.

is achieved. Fig. 18 shows the spectra of the upconverted signals. As it is difficult for the OF to select the positive first-order sidebands when the IF is low, the conversion efficiency is low when the frequency of the IF signal is lower than 2 GHz. When the IF is larger than 4 GHz, the powers of the

upconverted signals are significantly increased. The frequency of the upconverted signal is restricted by the bandwidth of the PD (~30 GHz in this experiment).

IV. Discussion

For most microwave photonic mixers, the inherent nonlinearity of the nonlinear medium will inevitably generate many undesirable sidebands. These sidebands together with the residual optical carrier and the desired sidebands would beat with each other at the PD to produce a considerable amount of mixing spurs with frequencies of $n\omega_S \pm m\omega_L$ $(n, m = 0, 1, 2, \ldots)$. The existence of mixing spurs would restrict the operational bandwidth of the frequency mixer. In the proposed reconfigurable frequency mixer, the suppression of mixing spurs is highly dependent on the purity of the first-order sidebands generated by the CS-SSB modulators. So far, the CS-SSB modulator has been implemented by a conventional intensity or phase modulator together with an optical bandpass filter or a commercially available DPMZM. For the filter-based approach, an OF with a large edge slope can be used to select the desired sideband while largely suppressing the undesirable optical carrier and sidebands, and for the DPMZM-based method, a high extinction-ratio DPMZM has been reported, which can achieve a suppression ratio of the undesired optical components as large as 47 dB [27]. If this DPMZM is applied, the mixing spurs will be very small.

If there are considerable undesirable sidebands (taking positive first-order sidebands as examples) existing in the optical signals, (1) and (2) can be rewritten as

$$E_S = -\sqrt{\frac{P_{\text{in}}}{2}}\sqrt{t_{\text{ff1}}}\sqrt{G_1}J_1(\beta_S) \times[\exp[j(\omega_c - \omega_S)t] + \alpha\exp[j(\omega_c + \omega_S)t]] \quad (11)$$

$$E_L = \pm\sqrt{\frac{P_{\text{in}}}{2}}\sqrt{t_{\text{ff2}}}\sqrt{G_2}J_1(\beta_L) \times[\exp[j(\omega_c - \omega_L)t] + \beta\exp[j(\omega_c + \omega_L)t]] \quad (12)$$

where α and β are the suppression ratios of the undesirable sidebands by the OFs in the two branches, respectively. After photodetection, the undesirable mixing spurs are given by

$$\begin{aligned} i_1 &= \alpha\frac{P_{\text{in}}}{2}\Re t_{\text{ff1}}G_1[J_1(\beta_S)]^2\cos(2\omega_S)t \\ i_2 &= \beta\frac{P_{\text{in}}}{2}\Re t_{\text{ff2}}G_2[J_1(\beta_L)]^2\cos(2\omega_L)t \\ i_3 &= (\alpha+\beta)\frac{P_{\text{in}}}{2}\Re\sqrt{t_{\text{ff1}}t_{\text{ff2}}}\sqrt{G_1G_2}J_1(\beta_S)J_1(\beta_L) \\ &\quad\times\cos(\omega_S + \omega_L)t. \end{aligned} \quad (13)$$

As can be seen, if α and β are sufficiently small, the powers of the mixing spurs would be quite small compared with that of the desirable frequency-converted components.

In the experiment, since the OFs we used have high edge slopes, only the two useful first-order sidebands are selected in the two branches. Therefore, after photodetection, only the desired frequency-converted components are generated, and the mixing spurs are effectively reduced, which can be confirmed by the electrical spectra shown in Figs. 12 and 18.

The performance of the OFs would affect not only the suppression of mixing spurs but also the frequency range of the proposed mixer. The lower bound of the frequency range of the proposed mixer is related to the roll-off slope of the OFs in the two branches. If the edge slope of the OF is k dB/nm and the minimum unwanted sideband suppression ratio is a dB, the minimum operation frequency of the proposed mixer is calculated to be $125a/k$, where the factor 125 is given because 1-nm bandwidth at 1550 nm corresponds to 125 GHz in frequency [31]. Since the bandwidths of the commercially available OFs can easily cover the entire C-band, the upper bound of the operational bandwidth is restricted mainly by the bandwidths of the electro-optical devices, i.e., the modulators and the PDs. Because wideband OFs are used, one may concern the influences of the undesired second-order sidebands located in the passbands of the OFs. However, the second-order sidebands will also be suppressed thanks again to the carrier suppression modulation. Therefore, wideband OFs with high roll-off factors are highly desired in the proposed mixer to achieve wideband photonic microwave mixing.

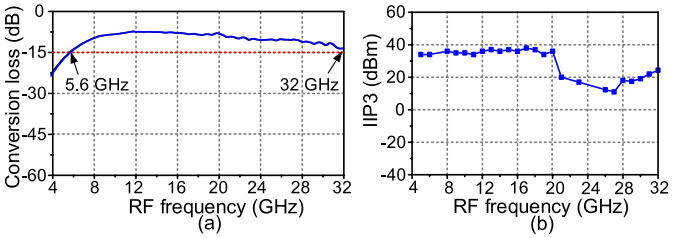

Fig. 19. Measured (a) bandwidth of the RF/IF port and LO port and (b) IIP3 within the operational bandwidth.

In the proposed mixer, since the roll-off factors of the filters are about 500 dB/nm, to maintain more than 20 dB unwanted sidebands suppression ratio, the lower bound of the mixer's bandwidth is about 5 GHz. The upper bound of the bandwidth of the proposed mixer is limited by the bandwidth of the PDs and modulators used in the experiment, which is about 32 GHz. The measured bandwidth of the RF/IF port and the LO port is shown in Fig. 19(a). It is measured by a 67-GHz electrical vector network analyzer (R&S ZVA67) by adjusting the frequencies of the RF and LO signals to make the IF fixed at 100 MHz. The power of the LO signal is 10 dBm. As can be seen, within the frequency range of 5.6–32 GHz, the conversion loss is below 15 dB, which means the bandwidth of the RF/IF port and the LO port is about 5.6–32 GHz (agrees with the analysis above). Besides, the IIP3 within this operational bandwidth is also measured and shown in Fig. 19(b). The lower IIP3 in the higher frequency range may be due to the nonlinearity of the electrical amplifier inside of the two-tone signal generator.

Since the sidebands in the lower and upper branches have different wavelengths, they cannot interfere with each other at the optical hybrid. This will result in a stable magnitude of the converted signal. In addition, although the environment variation will introduce considerable phase jitter to the converted signal, it can be compensated by using a feedback control method based on digital signal processing [32]. In our experiment, the system worked at room temperature over

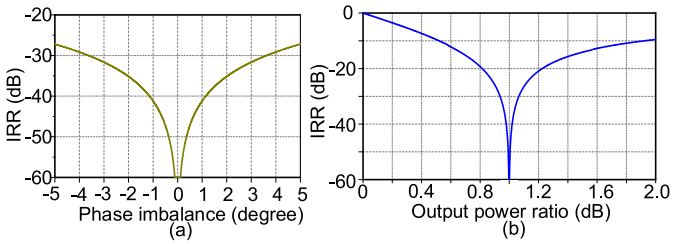

Fig. 20. Simulated IRR versus (a) phase imbalance and (b) output power ratio of the optical hybrid.

TABLE I
PERFORMANCE COMPARISON BETWEEN THE PROPOSED MIXER AND THE PREVIOUSLY REPORTED MIXERS

	CE [dB]	NF [dB]	SFDR [dB·Hz$^{2/3}$]	IRR [dB]	Function
This work	-15	20	120	60	reconfigurable
[3]	<-50	34	NA		single-ended
[7]	1.5-3	NA	NA		single-ended
[9]	11.5	NA	85.7		single-ended
[13]	-72	NA	NA		single-ended
[14]	7.8	23.5	115.6		single-ended
[15]	13.3	NA	NA		single-ended
[16]	~9	23	115		single-ended
[17]	>8	NA	NA		single-ended
[19]	NA	NA	114		single-ended
[20]	-15	31.8	127		single-ended
[25]	NA	NA	NA		I/Q
[26]	-40	NA	NA	>20	Balance/IRM
[27]	NA	NA	NA	NA	IRM
[28]	3-8	<20	106	150	IRM

BW: bandwidth; CE: conversion efficiency; NF: noise figure; SFDR: spurious free dynamic range; IRM: image-reject mixer, IRR: image-reject ratio

a duration of several hours. The power fluctuation of the converted signal is less than 0.3 dB.

It is well known that to achieve the I/Q and image-rejected mixing, quadrature phase shifts should be introduced to the LO or RF/IF signals, which is conventionally realized using one or more electrical 90° hybrid couplers [25]–[28]. In the proposed mixer, however, the quadrature phase shifts are equivalently implemented by the 90° optical hybrid. No operation is needed to the LO or RF/IF signals, which makes the system simpler. Although an electrical hybrid is still needed to implement the image-rejected mixing in the proposed mixer, it is operated at the IF band, which has a low frequency. As the quadrature phase shift is introduced by the optical hybrid, the insertion loss difference and phase imbalance of the optical hybrid become the main factors to influence the IRR of the image-reject mixer. Fig. 20 shows the image-rejection ratio versus the phase difference or the output power ratio of the optical hybrid. As can be seen from Fig. 20(a), if the insertion losses of the optical hybrid are identical, more than 35-dB IRR can be achieved for the phase imbalance within 2°. In addition, as can be seen from Fig. 20(b), the image-rejection ratio would be decreased as the amplitude imbalance increased. In practice, the phase imbalance of the optical hybrid is usually lower than that of the electrical quadrature hybrid. For example, the phase imbalance of the commercially available optical hybrid is within ±5° (typ. ±2°), but that of the electrical quadrature hybrid coupler is around ±10°.

Table I lists the performance comparison between the proposed mixer and the previously reported mixers in the literature. Compared with the previously reported methods, the proposed mixer has several advantages. First, unlike the photonic mixers in [3], [6]–[11], and [13]–[21], which can only achieve single-ended frequency mixing, the proposed mixer can realize reconfigurable mixing functions. In addition, for I/Q mixing, the conventional high-frequency electrical 90° hybrid coupler in [25]–[27] is replaced by the optical 90° hybrid in the proposed mixer, which results in a large bandwidth and low phase-imbalance. Besides, since the optical sidebands selection is employed to achieve the reconfigurable mixing functions, the mixing spurs suppression is high.

V. CONCLUSION

In this paper, we have reported and comprehensively studied a reconfigurable microwave photonic frequency mixer based on a 90° optical hybrid. According to the analysis, single-ended, double-balanced, I/Q, and image-reject mixing functions can all be performed with a common configuration but with different detection schemes. A theoretical analysis on the mixer is performed, and an experiment is carried out. The conversion efficiency is measured to be −10 dB and the SFDRs of the proposed photonic frequency mixer when implementing the downconversion and upconversion is 120 and 116 dBc · Hz$^{2/3}$, respectively. In addition, the measured image-rejection ratio when performing the frequency downconversion is about 60 dB. The reconfigurable mixer has the advantages of high mixing spur suppression, high RF and LO isolation, and good flexibility, which can find applications in radar or communication systems.

REFERENCES

[1] B. Cabon, "Microwave photonics mixing," *Sci. Iranica. Trans. D, Comput. Sci. Eng., Elect. Eng.*, vol. 17, no. 2, pp. 149–162, 2010.
[2] M. E. Manka, "Microwave photonics for electronic warfare applications," in *Proc. Int. Top. Meeting Microw. Photon. (MWP), 3rd Asia–Pacific Microw. Photon. Conf. (APMP)*, 2008, pp. 275–278.
[3] A. C. Lindsay, G. A. Knight, and S. T. Winnall, "Photonic mixers for wide bandwidth RF receiver applications," *IEEE Trans. Microw. Theory Techn.*, vol. 43, no. 9, pp. 2311–2317, Sep. 1995.
[4] B. Benazet, M. Sotom, M. Maignan, and J. Perdigues, "Microwave photonics cross-connect repeater for telecommunication satellites," *Proc. SPIE*, vol. 6194, p. 619403, Apr. 2006.
[5] S. Pan *et al.*, "Satellite payloads pay off," *IEEE Microw. Mag.*, vol. 16, no. 8, pp. 61–73, Sep. 2015.
[6] G. Maury, A. Hilt, T. Berceli, B. Cabon, and A. Vilcot, "Microwave-frequency conversion methods by optical interferometer and photodiode," *IEEE Trans. Microw. Theory Techn.*, vol. 45, no. 8, pp. 1481–1485, Aug. 1997.
[7] H.-J. Song, M. Park, H. J. Kim, J. S. Lee, and J.-I. Song, "All-optical frequency down-conversion for full-duplex WDM RoF systems utilizing an SOA-MZI," in *Proc. Int. Top. Meeting Microw. Photon. (MWP)*, 2005, pp. 321–324.
[8] R. Schnabel *et al.*, "Polarization insensitive frequency conversion of a 10-channel OFDM signal using four-wave-mixing in a semiconductor laser amplifier," *IEEE Photon. Technol. Lett.*, vol. 6, no. 1, pp. 56–58, Jan. 1994.
[9] C. Bohemond, T. Rampone, and A. Sharaiha, "Performances of a photonic microwave mixer based on cross-gain modulation in a semiconductor optical amplifier," *J. Lightw. Technol.*, vol. 29, no. 16, pp. 2402–2409, Aug. 15, 2011.

[10] S. Fu, W.-D. Zhong, P. Shum, Y. J. Wen, and M. Tang, "Simultaneous multichannel photonic up-conversion based on nonlinear polarization rotation of an SOA for radio-over-fiber systems," *IEEE Photon. Technol. Lett.*, vol. 21, no. 9, pp. 563–565, May 1, 2009.
[11] B. H. Kolner and D. W. Dolfi, "Intermodulation distortion and compression in an integrated electrooptic modulator," *Appl. Opt.*, vol. 26, no. 17, pp. 3676–3680, Sep. 1987.
[12] H. C. Yeh, C. H. Peng, B. Y. Lin, and H. C. Chang, "Modal analysis of plasmonic waveguides," in *Jpn.–Indo Workshop Microw., Photon., Commun. Syst. Dig.*, Fukuoka, Japan, Jul. 2007, pp. 94–98.
[13] G. K. Gopalakrishnan, W. K. Burns, and C. H. Bulmer, "Microwave-optical mixing in $LiNbO_3$ modulators," *IEEE Trans. Microw. Theory Techn.*, vol. 41, no. 12, pp. 2383–2391, Dec. 1993.
[14] E. H. W. Chan and R. A. Minasian, "Microwave photonic downconverter with high conversion efficiency," *J. Lightw. Technol.*, vol. 30, no. 23, pp. 3580–3585, Dec. 1, 2012.
[15] E. H. W. Chan, "Microwave photonic mixer based on a single bidirectional Mach–Zehnder modulator," *Appl. Opt.*, vol. 53, no. 7, pp. 1306–1314, Feb. 2014.
[16] E. H. W. Chan and R. A. Minasian, "Microwave photonic downconversion using phase modulators in a Sagnac Loop Interferometer," *IEEE J. Sel. Topics Quantum Electron.*, vol. 19, no. 6, pp. 211–218, Nov. 2013.
[17] C. Middleton, S. Meredith, R. Peach, and R. DeSalvo, "Photonic-based low phase noise frequency synthesis for RF-to-millimeter wave carriers and wideband RF-to-IF down-conversion," in *Proc. Military Commun. Conf. (MILCOM)*, Nov. 2011, pp. 51–54.
[18] C. Middleton, S. Meredith, R. Peach, and R. DeSalvo, "Photonic frequency conversion for wideband RF-to-IF down-conversion and digitization," in *Proc. IEEE Avionics, Fiber-Opt. Photon. Technol. Conf. (AVFOP)*, Oct. 2011, pp. 115–116.
[19] V. R. Pagán, B. M. Haas, and T. E. Murphy, "Linearized electrooptic microwave downconversion using phase modulation and optical filtering," *Opt. Exp.*, vol. 19, no. 2, pp. 883–895, Jan. 2011.
[20] A. Altaqui, E. H. W. Chan, and R. A. Minasian, "Microwave photonic mixer with high spurious-free dynamic range," *Appl. Opt.*, vol. 53, no. 17, pp. 3687–3695, Jun. 2014.
[21] Z. Tang, F. Zhang, D. Zhu, X. Zou, and S. Pan, "A photonic frequency downconverter based on a single dual-drive Mach–Zehnder modulator," in *Proc. Int. Top. Meeting Microw. Photon. (MWP)*, 2013, pp. 150–153, paper W4-8.
[22] Z. Tang, F. Zhang, and S. Pan, "Photonic microwave downconverter based on an optoelectronic oscillator using a single dual-drive Mach–Zehnder modulator," *Opt. Exp.*, vol. 22, no. 1, pp. 305–310, Jan. 2014.
[23] S. A. Maas, *Microwave Mixers*, vol. 1. Norwood, MA, USA: Artech House, 1986, p. 368.
[24] B. C. Henderson and J. A. Cook, "Image-reject and single-sideband mixers," Watkins-Johnson Co., Palo Alto, CA, USA, Tech. Rep. no. 18, 1985.
[25] V. R. Pagán and T. E. Murphy, "Electrooptic millimeter-wave downconversion and vector demodulation using phase-modulation and optical filtering," in *Proc. IEEE Avionics, Fiber-Opt. Photon. Technol. Conf. (AVFOP)*, Nov. 2014, pp. 13–14.
[26] H. Ogawa and H. Kamitsuna, "Fiber optic microwave links using balanced laser harmonic generation, and balanced/image cancellation laser mixing," *IEEE Trans. Microw. Theory Techn.*, vol. 40, no. 12, pp. 2278–2284, Dec. 1992.
[27] L. Chao, C. Wenyue, and J. F. Shiang, "Photonic mixers and image-rejection mixers for optical SCM systems," *IEEE Trans. Microw. Theory Techn.*, vol. 45, no. 8, pp. 1478–1480, Aug. 1997.
[28] S. J. Strutz and K. J. Williams, "A 0.8–8.8-GHz image rejection microwave photonic downconverter," *IEEE Photon. Technol. Lett.*, vol. 12, no. 10, pp. 1376–1378, Oct. 2000.
[29] Z. Tang and S. Pan, "A reconfigurable photonic microwave mixer," in *Proc. Int. Topical Meeting Microw. Photon. (MWP), 9th Asia–Pacific Microw. Photon. Conf. (APMP)*, Oct. 2014, pp. 343–345.
[30] Y. Yamaguchi, A. Kanno, T. Kawanishi, M. Izutsu, and H. Nakajima, "Pure single-sideband modulation using high extinction-ratio parallel Mach–Zehnder modulator with third-order harmonics superposition technique," in *Proc. CLEO, QELS_Fundam. Sci.*, 2015, p. JTh2A.40.
[31] Z. Tang, S. Pan, and J. Yao, "A high resolution optical vector network analyzer based on a wideband and wavelength-tunable optical single-sideband modulator," *Opt. Exp.*, vol. 20, no. 6, pp. 6555–6560, Mar. 2012.
[32] S. R. O'Connor, M. C. Gross, M. L. Dennis, and T. R. Clark, "Experimental demonstration of RF photonic downconversion from 4–40 GHz," in *Proc. Int. Top. Meeting Microw. Photon. (MWP)*, 2009, pp. 1–3.

Zhenzhou Tang (GSM'13) received the M.S. degree in information engineering from the Nanjing University of Aeronautics and Astronautics, Nanjing, China, in 2014, where he is currently pursuing the Ph.D. degree at the Key Laboratory of Radar Imaging and Microwave Photonics, Ministry of Education.

His current research interests include photonic generation of microwave signals and microwave photonic mixing.

Shilong Pan (S'06–M'09–SM'13) received the B.S. and Ph.D. degrees in electronics engineering from Tsinghua University, Beijing, China, in 2004 and 2008, respectively.

He was a "Vision 2010" Post-Doctoral Research Fellow with the Microwave Photonics Research Laboratory, University of Ottawa, ON, Canada, from 2008 to 2010. He joined the College of Electronic and Information Engineering, Nanjing University of Aeronautics and Astronautics, Nanjing, China, in 2010, where he is currently a Full Professor and an Executive Director of the Key Laboratory of Radar Imaging and Microwave Photonics with the Ministry of Education. He has authored or co-authored over 250 research papers, including over 130 papers in peer-reviewed journals and 120 papers in conference proceedings. His current research interests include microwave photonics, optical generation and processing of microwave signals, ultra-wideband over fiber, photonic microwave measurement, and integrated microwave photonics.

Dr. Pan is a Senior Member of the IEEE Microwave Theory and Techniques Society, the IEEE Photonics Society, and the IEEE Instrumentation and Measurement Society. He is a Member of the Optical Society of America. He is currently a Topical Editor of *Chinese Optics Letters*. He was a Chair of numerous international conferences and workshops, including the TPC Chair of the International Conference on Optical Communications and Networks in 2015, the High-Speed and Broadband Wireless Technologies Subcommittee of the IEEE Radio Wireless Symposium in 2013, 2014, and 2016, and the Optical Fiber Sensors and Microwave Photonics Subcommittee, and the Chair of the OptoElectronics and Communication Conference in 2015 and the Microwave Photonics for Broadband Measurement Workshop of the International Microwave Symposium in 2015. He was the recipient of an OSA Outstanding Reviewer Award in 2015.